

Fast and High-Quality Image Denoising via Malleable Convolutions

Yifan Jiang^{1,2*}, Bart Wronski¹, Ben Mildenhall¹, Jon Barron¹, Zhangyang Wang², Tianfan Xue¹

¹Google Research, ²University of Texas at Austin

Abstract

Many image processing networks apply a single set of static convolutional kernels across the entire input image, which is sub-optimal for natural images, as they often consist of heterogeneous visual patterns. Recent works in classification, segmentation, and image restoration have demonstrated that dynamic kernels outperform static kernels at modeling local image statistics. However, these works often adopt per-pixel convolution kernels, which introduce high memory and computation costs. To achieve spatial-varying processing without significant overhead, we present **Malleable Convolution (MalleConv)**, as an efficient variant of dynamic convolution. The weights of MalleConv are dynamically produced by an efficient predictor network capable of generating content-dependent outputs at specific spatial locations. Unlike previous works, MalleConv generates a much smaller set of spatially-varying kernels from input, which enlarges the network’s receptive field and significantly reduces computational and memory costs. These kernels are then applied to a full-resolution feature map through an efficient slice-and-conv operator with minimum memory overhead. We further build an efficient denoising network using MalleConv, coined as **MalleNet**. It achieves high quality results without very deep architecture, e.g., reaching $8.91\times$ faster speed compared to the best performed denoising algorithms (SwinIR), while maintaining similar performance. We also show that a single MalleConv added to a standard convolution-based backbone can contribute significantly to reducing the computational cost or boosting image quality at a similar cost. Project page: <https://yifanjiang.net/MalleConv.html>

1. Introduction

Image denoising is fundamental to the study of imaging and computer vision. Recent advances in deep learning have sparked significant interest in learning an end-to-end mapping directly from corrupted observations to the unobserved clean signal, without explicit statistical modeling of signal corruptions. These networks appear to learn a prior

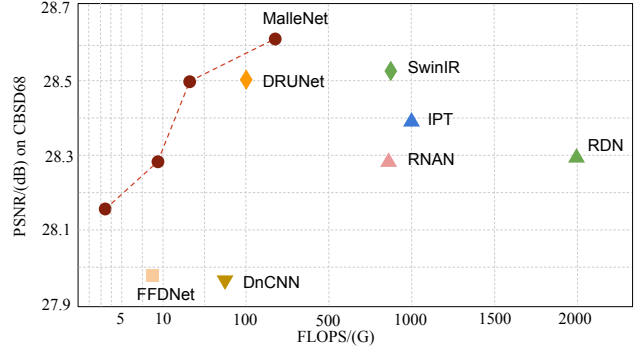


Figure 1. **Main results on CBSD68 test set ($\sigma = 50$).** Compared to other state-of-the-art models, our proposed MalleNet architecture achieves a better trade-off between quality and speed.

over the appearance of “ground truth” noiseless images in addition to the statistical properties of the noise present in the input images.

To better model image statistics, recent denoising networks consistently benefit from the addition of deeper and wider layers. This helps to both extract richer representations and to increase size of the network’s local receptive field. However, deeper and wider layers also significantly increases the computational costs and complexity of optimization.

One limitation is that most networks only use one set of convolutional kernels for the entire image, while natural images often contain spatially varying visual patterns. Recently, researchers address this issue by adopting a parameter prediction network (a.k.a. “hypernetwork”) [30, 26, 56, 45, 59] to generate per-pixel kernels at each specific location. Compared to static filters, generating spatially-varying filters via hypernetworks can significantly increase memory usage due to the large number of additional gradients and intermediate feature maps (Fig. 2(b)). Later works [36] generate dynamic filters by applying a channel-to-spatial transformation to each pixel without the need for a hypernetwork, *i.e.*, a spatial-specific and channel-agnostic approach (Fig. 2(c)). However, those methods failed to capture context and non-local information, due to the limited receptive field of the channel-to-spatial transformation.

To overcome these limitations, we propose an efficient implementation of spatially varying kernels, dubbed Malleable Convolution (**MalleConv**). Our intuition stems from

*This work was performed while Yifan Jiang worked at Google.

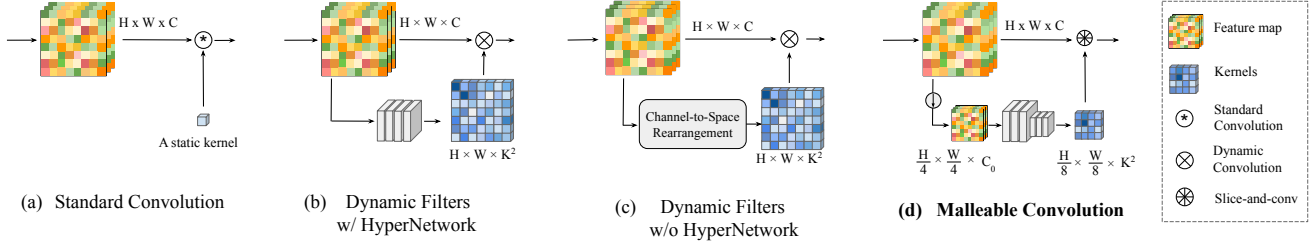


Figure 2. **Comparison with previous dynamic filters.** (a) Standard convolution with a static kernel. (b) Using a HyperNetwork to generate spatially-varying filters that replace static weights [26, 30]. (c) Generating dynamic filters a channel-to-space operation [36]. (d) Our proposed Malleable Convolution.

the trade-off between local smoothness and the global spatial heterogeneity. Fundamentally, natural images contain spatially-varying patterns in a “global” view, which motivates the popularity of dynamic filters [30, 26] and self-attention modules [55, 38]. Meanwhile, in a “local” neighborhood, the image contents are usually smoothly varying. In a broader sense, natural image patches tend to redundantly recur many times inside the image, both within the same scale and across different scales [48, 21]. Natural image textures are also commonly represented as a fractal set with self-similarity at all scales [33].

In contrast to previous approaches, the proposed MalleConv operation is positioned in a sweet spot between global heterogeneity and local smoothness by scaling the per-pixel dynamic filter approach to a larger region. Concretely speaking, MalleConv only processes a downsampled representation through a predictor network, and outputs location-specific dynamic filters at a much smaller spatial resolution (Fig. 2(d)). These kernels are later applied to full-resolution feature map through an memory-friendly slicing strategy, which combines bilinear slicing and convolution in a single operator. This design has several advantages. First, per-pixel kernels are calculated on-fly without additional memory I/O. Therefore, it significantly reduces the computational overhead. Second, unlike the hypernetwork used in dynamic filters, ours predictor network only takes a low-resolution feature map as input, so it is lightweight. Moreover, by taking a downsampled image as input, the predictor network has a large receptive field without very deep structure. As result, MalleConv both boost execution speed and improves quality, as shown in Fig. 1.

In summary, our contributions are outlined below:

- We propose Malleable Convolution (MalleConv), a new spatially-varying kernel that serves as a powerful variants of standard convolution. MalleConv largely benefits from an efficient predictor network, which incurs minimum additional cost when swapped into any existing network architecture.
- We conduct a comprehensive ablation study by inserting MalleConv into various popular backbone archi-

tectures (including DnCNN, UNet, RDN), where we show MalleConv can improve runtime by up to $20\times$.

- We compare MalleConv with previous spatially-varying kernel architectures including HyperNetworks [26], and Involution [36]. MalleConv demonstrates a better performance-efficiency trade-off.
- We further design a new MalleNet architecture using the proposed MalleConv block and it achieves fast and better performance on denoising tasks, on both synthetic and real-world benchmarks.

2. Related Work

Image Denoising Image denoising is a longstanding task in image processing and computer vision. Traditional image denoising algorithms utilize the neighboring information, like anisotropic diffusion [47] and total variation minimization [50]. Another line of works use sparse image priors, including the sparse coding [3, 17, 44], non-local means [6], filter banks [19], 3D transform filtering (BM3D) [13]. Recently, deep convolutional networks have demonstrated success in many image restoration tasks [15, 40, 70, 53, 34, 35, 49, 37, 60, 32, 57]. Specifically for the image denoising task, Burger et al. [7] proposed a plain multi-layer perception model that achieves comparable performance as BM3D. Chen et al. [11] proposed a trainable nonlinear reaction diffusion model that learns to remove additive white gaussian noise (AWGN) by unfolding a fixed number of inference steps. Many following works further improve it by using more elaborate neural network architecture designs, including residual learning [65], dense network [70], non-local module [69, 9, 38], dilated convolution [46], and others [12, 63, 62, 10]. However, many of these approaches use heavy network structure and are often not impractical in mobile use cases. To tackle this issue, several recent works focus on fast image denoising, by either introducing self-guidance network [23] or increasing the nonlinear model capacity [22]. In contrast with those methods, our approach relies on spatially varying kernels, where parameters are dynamically generated by an efficient prediction network.

Dynamic Filters and Spatially Varying Kernels Convolutional neural networks producing dynamic kernels have been widely studied for a variety of applications. The pioneer works [30, 26] start from adopting a parameter-generating network to produce location-specific filters. These works directly produce spatially-varying weights for the whole convolutional layer, substantially increasing the memory requirements and computational cost of their approaches. Wang et al. [56] designed a feature upsampling module (CARAFE) that generates kernels and reassembling features inside a predefined nearby region. However, CARAFE is designed as a feature upsampling operator instead of a variant of convolution. The context-gated convolution [41, 71] adopts a gated module and channel/spatial interaction module to generate modified convolutional kernels. Although their filter weights are produced dynamically, they apply the same filter at different spatial locations. Another track of work [36] avoids using a hypernetwork by employing a channel-to-space rearrangement to generate location-specific filters. Without the help of a hypernetwork, this approach can not capture the local information and image context. While previously described approaches mainly adopt dynamic filters inside convolutional layers of deep dynamic networks, a different line of work [5] proposed to use a standard convolutional neural network to predict denoising kernels applied directly to the target image. Mildenhall et al. [45] extended this approach to burst denoising by predicting a separate set of weights for each image in a temporal sequence. HDRNet [20] uses a deep neural network to process the low-resolution input and apply the produced spatially-varying affine matrix to the full-resolution input by slicing a predicted bilateral grid. In contrast to these methods, our proposed Malleable Convolution applies an efficient predictor network to process a downsampled feature map, then constructs a deep spatially-varying network layer-by-layer.

3. Method

3.1. Preliminaries

A standard convolutional layer applies a kernel with weights $W \in \mathbb{R}^{C_{in} \times C_{out} \times K^2}$ to an input feature map sampled from a 2D tensor $X \in \mathbb{R}^{C_{in} \times H \times W}$. H, W are height and width of the feature map, C_{in}, C_{out} denote the numbers of input and output channels respectively, and K is the kernel size. In each output location, a local patch with size $C_{in} \times K^2$ around that location is collected from the input and multiplied with the kernel weight matrices W , and all output pixels share the same kernels. This basic design struggles to capture context information and cannot adapt to different regions of natural images that contain spatially heterogeneous patterns. Although previous works address this issue by adopting the per-pixel dynamic

filters [26, 30, 45] or generating spatial-agnostic filter via channel-to-space permutation [36], their approaches either require large memory footprint or can not capture context information.

3.2. Malleable Convolution with Efficient Predictor Network

To overcome the aforementioned drawbacks, we propose a new operation, dubbed Malleable Convolution (MalleConv). MalleConv is equipped with a light-weight predictor network that significantly reduces the memory cost and runtime latency of dynamic kernel prediction. Unlike the dynamic filter networks [30] or HyperNetworks [26], the proposed efficient predictor network first downsamples the input feature map X to $X' \in \mathbb{R}^{\frac{H}{4} \times \frac{W}{4} \times C}$ through a 4×4 average pooling. This downsampling both reduces the computational cost and also increases the receptive field of the generated filters.

After downsampling, we build a light-weight predictor network consists of multiple ResNet blocks [28] and max pooling layers [27] (see supplementary materials for detailed architecture). The predictor network outputs a feature map $Y \in \mathbb{R}^{\frac{H}{8} \times \frac{W}{8} \times C'}$, where $C' = K^2 \times C$. To formulate a spatially-varying filter, the learned representation Y is reshaped to a list of filters $\{W_{ij}\} \in \mathbb{R}^{K^2 \times C}$, where $i \in \{1, 2, \dots, \frac{H}{8}\}$, $j \in \{1, 2, \dots, \frac{W}{8}\}$. Each kernel in Y only has C channels, not $C_{in} \times C_{out}$, as we use the depth-wise convolution [29] to further reduce the size of parameters. Finally, we upsample the learned spatially-varying filters $\{W_{ij}\}$ through bilinear interpolation and to obtain per-pixel filters $\{W'_{ij}\} \in \mathbb{R}^{K^2 \times C}$, where $i \in \{1, 2, \dots, H\}$, $j \in \{1, 2, \dots, W\}$, and independently apply them to the corresponding input channels.

3.3. Efficient Slice-and-Conv Operator

A naive way to implement malleable convolution is to first upsample the low-resolution filters to full-resolution using bilinear interpolation and then applies the feature map. However, this introduces a large memory footprint by storing a full-resolution kernels.

To mitigate the memory issue, we combine these two steps into a slicing-and-conv operator. It takes in a feature map $X \in \mathbb{R}^{H \times W \times C}$ and a lower resolution kernel maps $\{W_{ij}\} \in \mathbb{R}^{K^2 \times C}$ as input. The result of the slicing-and-conv operator is a new feature map Z with the same resolution as X . For each pixel location, we first calculate the bilinear interpolated kernel weights from four neighboring kernels as (also illustrated in bottom right of Fig. 3)

$$W'_{x,y} = \sum_{i,j \in N(x,y)} \tau(r_x x - i) \tau(r_y y - j) W'_{i,j}, \quad (1)$$

where τ is the linear interpolation operator $\tau(a) = \max(1 - |a|, 0)$, r_x and r_y are the width and height ratios

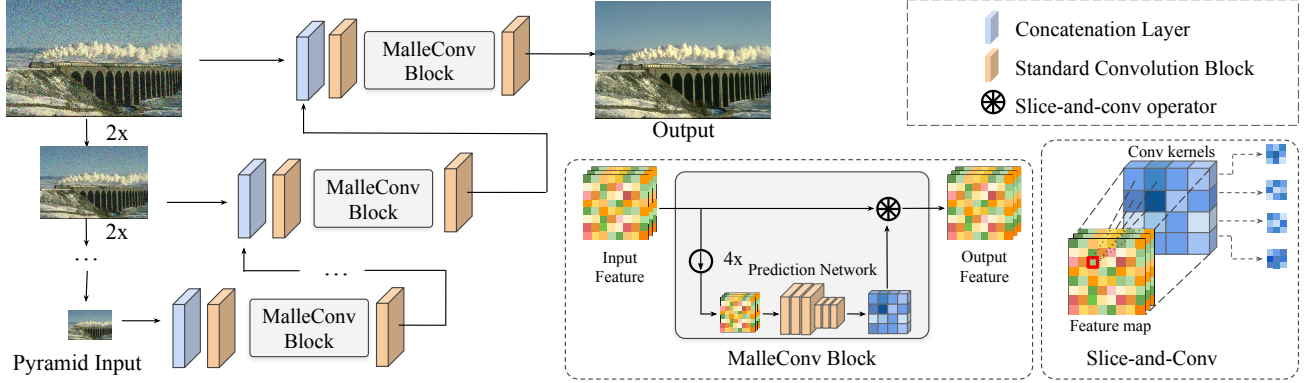


Figure 3. **Architecture of MalleNet.** MalleNet takes a 4-level pyramid as input and each layer consists of several Inverted Bottleneck Blocks with a MalleConv block inserted in between. Bottom middle shows the structure of MalleConv block, which consists of a small prediction network and a slice-and-conv operator. Bottom right shows details of slice-and-conv operator. For each input feature (red rectangle), four neighboring kernels are bilinearly combined and applied to that feature to generate the corresponding output feature.

of the low-resolution filters w.r.t. the full resolution input feature map, and $N(x, y)$ is the four-neighborhood. Bias term $b'_{x,y}$ is sliced in the similar way. The output feature Z is then calculated as:

$$Z_{x,y}(c) = W'_{x,y}(c) \cdot X_{x,y}(c) + b'_{x,y}(c), \quad (2)$$

where c is the channel index. Note that the sliced weight W' and bias b' are calculate on-the-fly without additional memory cost. We discuss more about the specific memory consumption in Sec. 5.3.

4. Malleable Network

As the goal of this work is to design an ultra-fast denoiser, current state-of-the-art algorithms, both the residual dense network [70] or the transformer-based architecture [9, 38] are sub-optimal to build an efficient backbone. Inspired by some recent pyramid-based approaches [39, 23, 62], we design a new backbone where the proposed malleable convolution is integrated, dubbed **MalleNet**.

MalleNet firstly build a four-level pyramid using $2 \times$ Space-to-Channel shuffle operation [52]. This allows us to extract multi-scale representations and further increases the network’s receptive field. In each stage, we stack several Inverted Bottleneck Blocks [51] with a fixed ratio, and inserted one 1×1 or 3×3 Malleable Convolution in between to extract the heterogeneous representations. At the end of the bottom stage, we upsample the feature map and concatenate it with the input of its upper stage. In the top stage, the representation extracted from different pyramids are aggregated to produce the final output. Compared to conventional encoder-decoder style architectures, the pyramid-based architecture reuses the extracted representation from each scale and thus can achieve faster inference speed. The whole network is shown in Fig. 3.

5. Experiments

We benchmark the proposed module on the Additive White Gaussian Noise (AWGN) removal task. Following previous work [64], we construct a training dataset with 400 examples from Berkeley segmentation dataset (BSD), 4,744 examples from Waterloo Exploration Database [43], 900 images from DIV2K dataset [2], and 2,750 images from Flick2K dataset [40]. The training examples are randomly cropped to 192×192 patches, which we augment through random rotations and flipping. We adopt Adam Optimizer with a batch size of 16 and a cosine learning rate scheduler. The initial learning rate is set to 0.001. The total training process takes 2.2M iterations.

We adopt 3 common datasets as our testing set: CBSD68, kodak24 [18], McMaster [68]. Following previous work, we conduct three experiments, where the training and test set is generated by adding Gaussian noise with $\sigma = 15, 25, 50$ to the clean images. As MalleConv is efficient enough, we do not need to crop (tile) the test examples into small patches like previous works [69, 9, 38], and can directly process the full-resolution test images.

All of our experiments are conducted on 8 Nvidia V100 GPUs and Tensorflow-2.6 platform. The FLOPs and runtime are calculated on 256×256 resolution RGB input. We also evaluate the runtime inference speed of these approaches, where the experiments are set on an Nvidia P6000 GPU platform with batch size set to the maximum available number. For PyTorch-based approaches, we report the average latency of a single $256 \times 256 \times 3$ input collected from 500 runs. For Tensorflow-based ones, we report the latency time using the Tensorflow official profiler.

5.1. Comparing with State-of-the-Art Methods

To fairly compare the runtime speed between MalleNet and other baselines, we train 4 versions of MalleNet: -XS,

Method	Latency/(ms)	Flops/(G)	CBSD68			Kodak24			McMaster		
			$\sigma = 15$	$\sigma = 25$	$\sigma = 50$	$\sigma = 15$	$\sigma = 25$	$\sigma = 50$	$\sigma = 15$	$\sigma = 25$	$\sigma = 50$
BM3D [13]	41.56	-	33.52	30.71	27.38	34.28	32.15	28.46	34.06	31.66	28.51
DnCNN [65]	21.69	68.15	33.90	31.24	27.95	34.60	32.14	28.95	33.45	31.52	28.62
FFDNet [67]	-	7.95	33.87	31.21	27.96	34.63	32.13	28.98	34.66	32.35	29.18
MalleNet-S	4.62	2.93	33.90	33.22	27.97	34.66	32.16	29.00	34.68	32.35	29.20
RPCNN [58]	95.11	-	-	31.24	28.06	-	32.34	29.25	-	32.33	29.33
DSNet [46]	-	-	33.91	31.28	28.05	34.63	32.16	29.05	34.67	32.40	29.28
IRCNN [66]	-	12.18	33.86	31.16	27.86	34.69	32.18	28.93	34.58	32.18	28.91
MalleNet-M	16.69	9.36	34.15	31.50	28.27	34.82	32.41	29.35	35.53	33.12	29.96
BRDNet [54]	-	-	34.10	31.43	28.16	34.88	32.41	29.22	35.08	32.75	29.52
DRUNet [64]	-	102.91	34.30	31.69	28.51	35.31	32.89	29.86	35.40	33.14	30.08
MalleNet-L	32.34	33.47	34.32	31.71	28.52	34.93	32.58	29.50	35.65	33.26	30.12
RNAN [69]	-	774.67	-	-	28.27	-	-	29.58	-	-	29.72
RDN [70]	263.03	2001.86	-	-	28.31	-	-	29.66	-	-	-
IPT [9]	-	938.66	-	-	28.39	-	-	29.64	-	-	29.98
SwinIR [38]	780.61	788.10	34.42	31.78	28.56	35.34	32.89	29.79	35.61	33/20	30.22
MalleNet-XL	87.55	181.89	34.43	31.82	28.62	35.23	32.65	29.61	35.70	33.28	30.23

Table 1. Comparing MalleNet with the state-of-the-art methods on three common benchmarks. We try our best to use the official implementation provided by the authors to calculate FLOPs and latency.

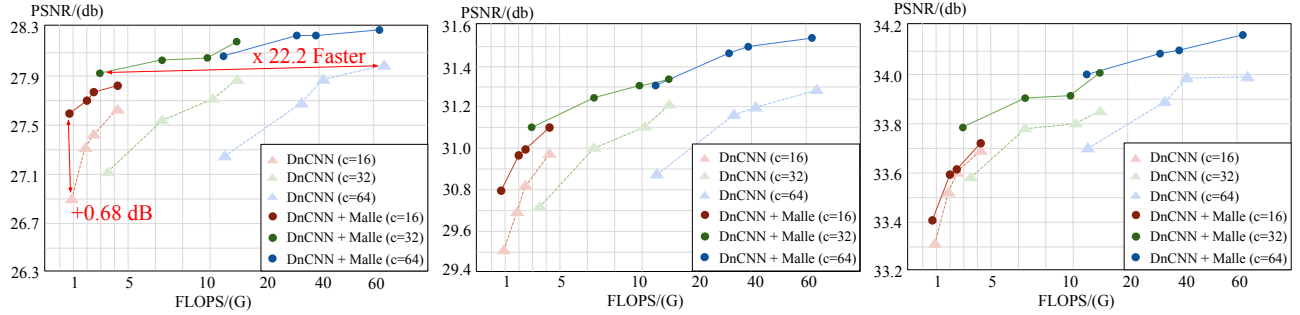


Figure 4. PSNR-To-Complexity trade-off of DnCNN and DnCNN with a single MalleConv. We build DnCNN-families by setting depth = {3, 6, 9, 15} and channel = {16, 32, 64}. The three figures from left to right show experiments with $\sigma = \{50, 25, 15\}$.

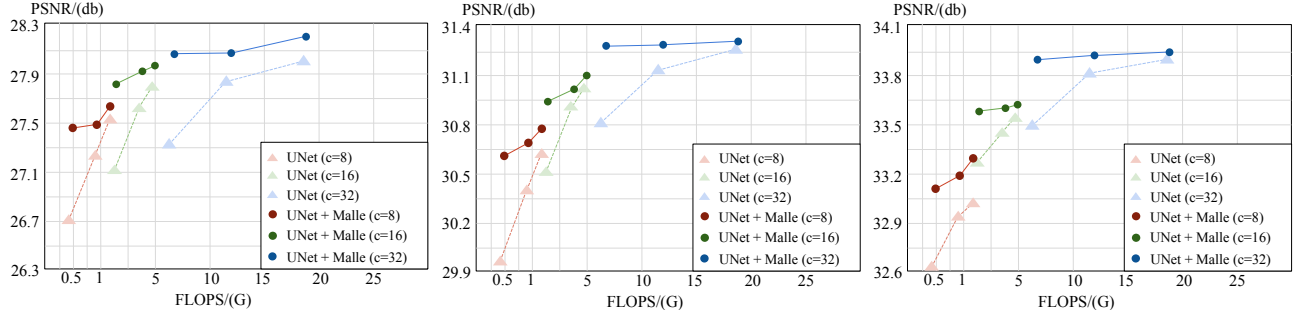


Figure 5. PSNR-To-Complexity trade-off of UNet and UNet with a single MalleConv. We build UNet-families by setting the encoder-decoder stage number = {2, 3, 4} and channel = {8, 16, 32}. The three figures show experiments with $\sigma = \{50, 25, 15\}$.

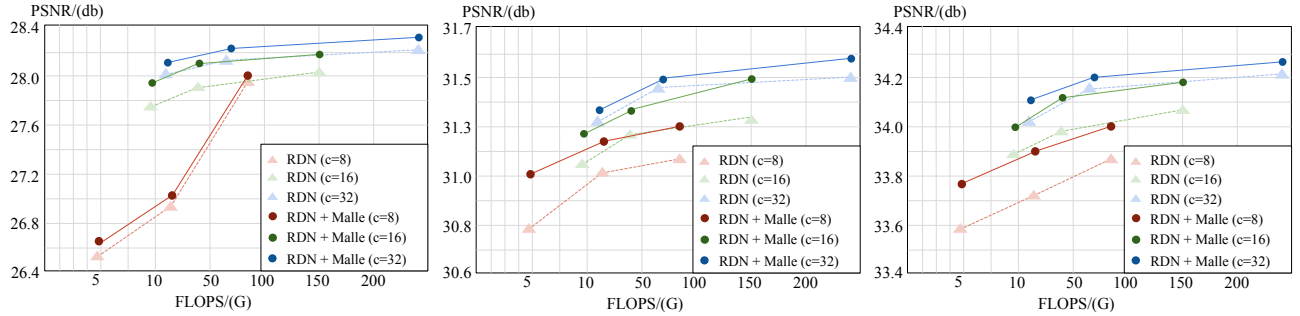


Figure 6. PSNR-To-Complexity trade-off of RDN and RDN with a single MalleConv. We build RDN-families by setting the residual dense block number = {3, 6, 10} and channel = {8, 16, 32}. The three figures show experiments with $\sigma = \{50, 25, 15\}$.

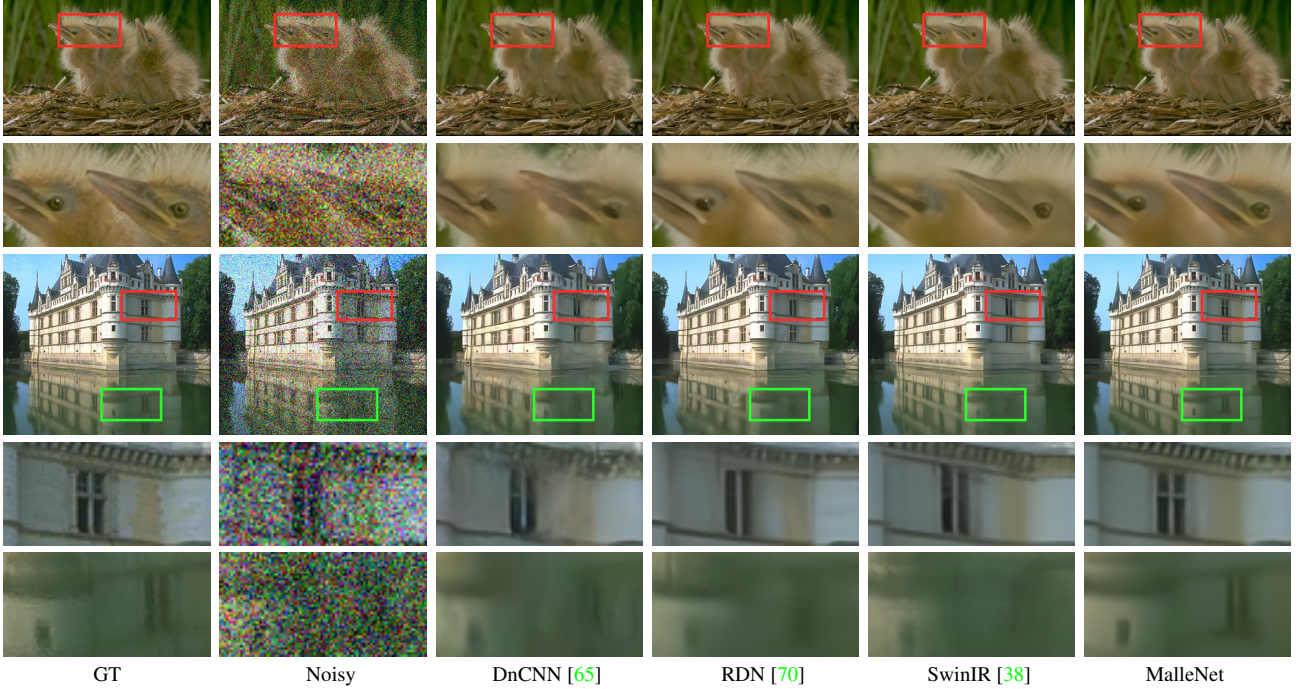


Figure 7. Visual comparison between MalleNet and previous approaches. More visual results are shown in the supplementary.

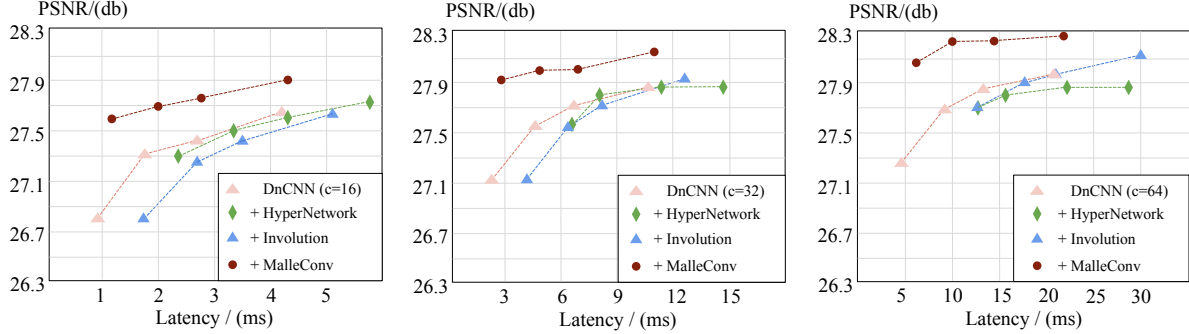


Figure 8. Comparison between MalleConv and other dynamic filters in terms of runtime latency and PSNR value.

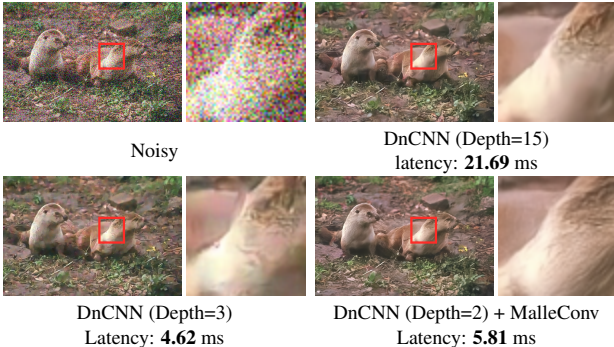


Figure 9. Visual results by injecting MalleConv to a fast variant of DnCNN, under the setting of $\sigma = 50$.

-S, -M, -L, and -XL by growing the channel from 16 to 128. For MalleNet-XS, we replace the inverted bottleneck block with a standard residual block as empirically it achieves better latency time in the “ultra-fast” setting. For MalleNet-

XL, we further increase the expansion ratio of the inverse bottleneck blocks from 3 to 5 for better quality. Detailed network configurations are included in the supplementary material.

We divide evaluated approaches into four categories according to their performance and runtime speed, shown in Table 1. The first group includes the most efficient approaches with very light backbones. The proposed MalleNet-XS achieves best performance on three test sets under three different settings ($\sigma = 15, 25, 50$), while it uses only **2.84 G** FLOPs. MalleNet-XS slightly outperforms the previous best methods FFDNet [67] while the computational costs is $\times 2.64$ smaller. Meanwhile, MalleNet-XL reaches $\times 4.69$ runtime speed-up when compared to DnCNN architecture. In the second runtime cost group, MalleNet-M significantly outperforms all baselines by up to **+0.94 dB** on McMaster dataset, while it only takes **9.36 G**

Depth	Metrics	AvgPooling Size			
		0	2	4	8
D=3	Latency/(ms)	13.19	7.08	5.62	5.18
	FLOPs/(G)	43.96	18.17	11.71	10.10
	PSNR/(dB)	27.91	28.15	28.07	28.01
D=6	Latency/(ms)	17.39	11.28	9.85	9.43
	FLOPs/(G)	62.05	36.26	29.81	28.19
	PSNR/(dB)	28.19	28.24	28.24	28.18
D=15	Latency/(ms)	30.09	23.98	22.53	22.09
	FLOPs/(G)	98.24	72.44	66.00	64.39
	PSNR/(dB)	28.25	28.28	28.31	28.28

Table 2. Ablation study on the size of AvgPooling layer in MalleConv Operator. PSNR results are reported on the CBSD68 test set with $\sigma = 50$.

FLOPs. In the third group, we evaluate a larger architecture MalleNet-L and compare it with two comparable baselines, BRDNet and DRUNet. MalleNet-M outperforms the best baseline DRUNet on two test sets CBSD68 and McMaster by up to **+0.25 dB** PSNR, while being slightly behind it on Kodak24 dataset. Considering its computational costs, MalleNet-M is able to speed up by $\times 3.07$ ratio as compared to DRUNet, showing its favorable computational efficiency.

In the last group, we collect two best-perform denoising algorithm IPT and SwinIR, powered by Vision Transformer [16]. Vision Transformer is known to be effective on various tasks [8, 42, 31, 72] with a high computational cost. The best performed algorithm SwinIR takes 780.61ms and consumes 788.10G FLOPs, which is impractical for edge devices. In contrast, MalleNet-XL is $\times 12.41$ faster and takes $\times 4.33$ less FLOPs, but still outperforms SwinIR on CBSD68 and McMaster dataset by a margin up to **+0.12 dB**, while performing slightly worse on the Kodak24 dataset. On these four categories, MalleNet achieves the best efficiency-performance trade-off and reaches state-of-the-art results among two of our main benchmark test sets.

5.2. MalleConv layer used in alternative backbones

To further demonstrate the effectiveness of the proposed Malleable Convolution operator, we set ablation studies by injecting MalleConv to existing well-known backbones, as a plug-in operator. Here we choose three popular backbones as our main testbeds, including the ResNet-style backbone (DnCNN [65]), UNet-style backbone, and DenseNet-style backbone (RDNet [70]). Since most of original network structures are too heavy for edge devices, we also manually build a few cheaper variants by controlling the depth and channel variables. Using DnCNN as an example, the vanilla DnCNN architecture contains 15 layers with 64 channels. We construct its faster version by setting the depth = {3, 6, 9, 15} and channel = {16, 32, 64}, respectively, and obtain the architecture series of DnCNN with $3 \times 4 = 12$ variants. We then are able to evaluate the efficiency-and-performance trade-off of these architecture families.

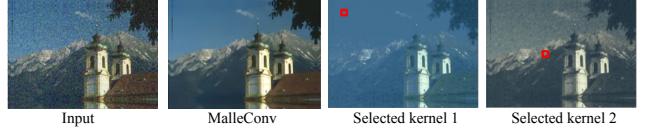


Figure 10. Comparison between default MalleConv output (column2) and outputs using two selected kernels (column 3 and 4).

Afterwards, we construct a number of better performing variants of these architecture series, **by replacing one standard convolution with a single 1×1 MalleConv operator**. We replace the middle layer of the network with a MalleConv block (detailed architectures are shown in the supplementary material). We conduct experiments on CBSD69 dataset and train these architectures using the same training recipes. As shown in Fig. 4, 5, and 6, a single MalleConv block brings significant improvement to all three backbones. For example, by decreasing the depth (d) and channel (c) of DnCNN from (d, c) = (15, 64) to (3, 16), one can obtain an ultra-fast variant of DnCNN. However, such an ultra-fast variant shows poor performance, e.g., only reaching 26.91 db on CBSD68 test set when $\sigma = 50$. In contrast to vanilla DnCNN, simplified DnCNN with MalleConv layer achieves significantly better performance (increased by **+0.68 dB**) while maintaining similar computational costs. Similarly, UNet-families with MalleConv and RDNet-families with MalleConv also show better PSNR-Complexity trade-off when compared to their vanilla versions, demonstrating the advantage of the proposed MalleConv block.

5.3. Visual Comparison and Interpretation

We first compare our best architecture MalleNet-XL with previous state-of-the-art approaches, including Residual Dense Network [70] and Swin Transformer based architecture [38], as shown in Fig. 7. The examples produced by MalleNet preserve rich details and impressive textures while saving up to $\times 8.91$ inference time compared to the best baseline, further demonstrating the effectiveness of our approach. Moreover, in the “ultra-fast” setting, we decrease the depth of DnCNN from 15 to 3 to obtain a much faster variant of DnCNN architecture. However, image quality also degrades as shown in the bottom-left of Fig. 9. In contrast, when replacing the middle layer of DnCNN with a single 1×1 MalleConv operator (DnCNN w/ MalleConv), it uses a slight more computational time, but achieves significantly better visual quality, as shown in the bottom-right of Fig. 9.

Furthermore, to illustrate how special-varying kernels in MalleConv capture heterogeneous visual patterns, we replace the spatially varying kernels in MalleNet with one selected kernel, and apply it to the entire image. Fig. 10 shows a comparison between the default output of MalleNet (column 2) with the one that applies a selected kernel (columns 3 and 4). When a kernel generated from a sky region (col-

Method	DnCNN [65]	BM3D [13]	WNNM [24]	CBDNet [25]	RIDNet [4]	VDN [61]	MPRNet [63]	NBNet [12]	MIRNet [62]	HINet [10]	MalleNet-R
Latency/(ms)	21.69	41.56	-	-	98.13	-	-	37.44	192.61	32.83	13.58
FLOPs/(G)	68.15	-	-	-	-	-	573.50	88.70	787.04	170.71	29.11
PSNR	23.66	25.78	25.78	30.78	38.71	39.28	39.17	39.75	39.72	39.99	38.05
SSIM	0.583	0.685	0.809	0.754	0.914	0.909	0.958	0.973	0.959	0.958	0.911

Table 3. **Comparing MalleNet with the State-of-the-art methods on real-world benchmark SIDD.** We try our best to use the official implementation provided by the authors to calculate the FLOPs cost and runtime speed.

umn 3) is applied, the network is observed to denoise the rest of the image as if they are the sky. Similarly, using a kernel from a snowy-mountain patch will generate output looks like snowy mountain (column 4). By combining kernels that are dedicated for different local image statistics together, MalleConv can better model the heterogeneous spatial patterns and yield better results.

5.4. Analysis of Runtime Latency

We also investigate the specific computational cost of each individual network equipped with MalleConv and other dynamic filters, e.g., HyperNetwork [26] and Involution [36]. We adopt DnCNN [65] as our main backbone and replace the middle layer of DnCNN with a single dynamic filter operator. We set up three experiments on DnCNN backbone with channel={16, 32, 64}. In each experiment, the depth of DnCNN backbone are growing from 3, 6, 9, to 15. As shown in Fig. 8, MalleConv achieves the best performance-and-efficiency trade-off by significantly improving the PSNR score with minimum additional runtime latency.

Moreover, we conduct the ablation study on the down-sampling ratio of the proposed efficient predictor network. Similar to the aforementioned setting, we set our testbed on DnCNN approach and examine three different architectures by setting depth = {3, 6, 15}. We evaluate the runtime speed, FLOPs cost, and PSNR value of four variants with the size of the AvgPooling layer equal to {0, 2, 4, 8}. As shown in Table 2, by processing a $4\times$ downsampled feature map, our proposed efficient predictor network achieves a “win-win” on both performance and efficiency.

5.5. Evaluation on Real Sensor Noise

At least, we evaluate our approaches to real sensor noise. Similar to previous works [12, 62], the Smartphone Image Denoising Dataset (SIDD) [1] is adopted as main benchmark. SIDD captures 30,000 noisy images from 10 scenes under different lighting conditions using five popular smartphone cameras and generated their ground truth images through a systematic procedure. During the training process, we randomly crop 448×448 patches and apply random rotation and flipping. We report the PSNR/SSIM score on SIDD validation set, which contains 1280 cropped patches. We train a real denoiser MalleNet-R, by slightly modifying the channel/depth of MalleNet-M architecture and

replace Inverse Bottleneck Block with standard residual block (see supplementary materials for details). As shown in Table 3, MalleNet-R achieves lower latency (**13.58 ms**) compared with other methods. In terms of image quality, MalleNet-R is able to reach similar PSNR/SSIM compared to most baselines, and only slightly behinds the approaches with very heavy computational cost or equipped with complex channel/spatial attention module. More visual comparisons are included in the supplementary materials.

6. Conclusions

In this work, we propose Malleable Convolution (MalleConv), an efficient variant of spatially-varying convolution tailored for ultra-fast image denoising. MalleConv processes a low-resolution feature map and generates a much smaller set of spatially varying filters. The generated filters inherently fit the heterogeneous and spatially varying patterns presented in natural images, while taking little additional computational costs. We conduct evaluation on multiple common benchmarks where MalleConv achieves state-of-the-art efficiency/performance trade-off. We also demonstrate the benefits of MalleConv by injecting it to several different common denoising network backbones.

Despite its effectiveness, we also observe that very deep or wide architectures benefit less from MalleConv, as they may also capture heterogeneous image statistics in a less efficient way. A future work is to augment MalleConv by other architectures, e.g., attention mechanism [38] or deformable shape [14], to further improve its quality in applications with less computational constraints.

Social Impact. Our technology focuses on world-positive use cases. The proposed denoising algorithm is focusing on reducing sensor noise without modifying actual image content, and experiments show the risk of introducing disinformation is low. However, we acknowledge the potential for misuse of the repurposing proposed algorithm for modifying image content. To that end, we strive the importance of clearly indicating the nature and intent of the processing when sharing visual content that has been processed by these techniques. Finally, we also believe it is crucial to be thoughtful and ethical about the content being processed. We follow these guiding principles in our work.

References

- [1] Abdelrahman Abdelhamed, Stephen Lin, and Michael S Brown. A high-quality denoising dataset for smartphone cameras. *CVPR*, 2018. 8
- [2] Eirikur Agustsson and Radu Timofte. Ntire 2017 challenge on single image super-resolution: Dataset and study. *CVPR workshops*, 2017. 4
- [3] Michal Aharon, Michael Elad, and Alfred Bruckstein. K-svd: An algorithm for designing overcomplete dictionaries for sparse representation. *IEEE Transactions on signal processing*, 2006. 2
- [4] Saeed Anwar and Nick Barnes. Real image denoising with feature attention. In *Proceedings of the IEEE/CVF International Conference on Computer Vision*, pages 3155–3164, 2019. 8
- [5] Steve Bako, Thijs Vogels, Brian McWilliams, Mark Meyer, Jan Novák, Alex Harvill, Pradeep Sen, Tony Derose, and Fabrice Rousselle. Kernel-predicting convolutional networks for denoising monte carlo renderings. *ACM Trans. Graph.*, 2017. 3
- [6] Antoni Buades, Bartomeu Coll, and J-M Morel. A non-local algorithm for image denoising. *CVPR*, 2005. 2
- [7] Harold C Burger, Christian J Schuler, and Stefan Harmeling. Image denoising: Can plain neural networks compete with bm3d? *CVPR*, 2012. 2
- [8] Nicolas Carion, Francisco Massa, Gabriel Synnaeve, Nicolas Usunier, Alexander Kirillov, and Sergey Zagoruyko. End-to-end object detection with transformers. *ECCV*, 2020. 7
- [9] Hanting Chen, Yunhe Wang, Tianyu Guo, Chang Xu, Yiping Deng, Zhenhua Liu, Siwei Ma, Chunjing Xu, Chao Xu, and Wen Gao. Pre-trained image processing transformer. *CVPR*, 2021. 2, 4, 5
- [10] Liangyu Chen, Xin Lu, Jie Zhang, Xiaojie Chu, and Chengpeng Chen. Hinet: Half instance normalization network for image restoration. *CVPR*, 2021. 2, 8
- [11] Yunjin Chen and Thomas Pock. Trainable nonlinear reaction diffusion: A flexible framework for fast and effective image restoration. *TPAMI*, 2016. 2
- [12] Shen Cheng, Yuzhi Wang, Haibin Huang, Donghao Liu, Haoqiang Fan, and Shuaicheng Liu. Nbnnet: Noise basis learning for image denoising with subspace projection. *CVPR*, 2021. 2, 8
- [13] Kostadin Dabov, Alessandro Foi, Vladimir Katkovnik, and Karen Egiazarian. Image denoising by sparse 3-d transform-domain collaborative filtering. *IEEE Transactions on image processing*, 2007. 2, 5, 8
- [14] Jifeng Dai, Haozhi Qi, Yuwen Xiong, Yi Li, Guodong Zhang, Han Hu, and Yichen Wei. Deformable convolutional networks. In *Proceedings of the IEEE international conference on computer vision*, pages 764–773, 2017. 8
- [15] Chao Dong, Chen Change Loy, Kaiming He, and Xiaoou Tang. Image super-resolution using deep convolutional networks. *TPAMI*, 2015. 2
- [16] Alexey Dosovitskiy, Lucas Beyer, Alexander Kolesnikov, Dirk Weissenborn, Xiaohua Zhai, Thomas Unterthiner, Mostafa Dehghani, Matthias Minderer, Georg Heigold, Sylvain Gelly, et al. An image is worth 16x16 words: Transformers for image recognition at scale. *arXiv:2010.11929*, 2020. 7
- [17] Michael Elad and Michal Aharon. Image denoising via sparse and redundant representations over learned dictionaries. *IEEE Transactions on Image processing*, 2006. 2
- [18] Rich Franzen. Kodak lossless true color image suite. *source: http://r0k.us/graphics/kodak*, 1999. 4
- [19] Pascal Getreuer, Ignacio Garcia-Dorado, John Isidoro, Sungjoon Choi, Frank Ong, and Peyman Milanfar. Blade: Filter learning for general purpose computational photography. In *2018 IEEE International Conference on Computational Photography (ICCP)*, pages 1–11. IEEE, 2018. 2
- [20] Michaël Gharbi, Jiawen Chen, Jonathan T. Barron, Samuel W Hasinoff, and Frédéric Durand. Deep bilateral learning for real-time image enhancement. *SIGGRAPH*, 2017. 3
- [21] Daniel Glasner, Shai Bagon, and Michal Irani. Super-resolution from a single image. *ICCV*, 2009. 2
- [22] Shuhang Gu, Wen Li, Luc Van Gool, and Radu Timofte. Fast image restoration with multi-bin trainable linear units. *ICCV*, 2019. 2
- [23] Shuhang Gu, Yawei Li, Luc Van Gool, and Radu Timofte. Self-guided network for fast image denoising. *ICCV*, 2019. 2, 4
- [24] Shuhang Gu, Lei Zhang, Wangmeng Zuo, and Xiangchu Feng. Weighted nuclear norm minimization with application to image denoising. *CVPR*, 2014. 8
- [25] Shi Guo, Zifei Yan, Kai Zhang, Wangmeng Zuo, and Lei Zhang. Toward convolutional blind denoising of real photographs. In *Proceedings of the IEEE/CVF Conference on Computer Vision and Pattern Recognition*, pages 1712–1722, 2019. 8
- [26] David Ha, Andrew Dai, and Quoc V Le. Hypernetworks. *arXiv:1609.09106*, 2016. 1, 2, 3, 8
- [27] Kaiming He, Xiangyu Zhang, Shaoqing Ren, and Jian Sun. Delving deep into rectifiers: Surpassing human-level performance on imagenet classification. *ICCV*, 2015. 3
- [28] Kaiming He, Xiangyu Zhang, Shaoqing Ren, and Jian Sun. Deep residual learning for image recognition. *CVPR*, 2016. 3
- [29] Andrew G Howard, Menglong Zhu, Bo Chen, Dmitry Kalenichenko, Weijun Wang, Tobias Weyand, Marco Andreetto, and Hartwig Adam. Mobilenets: Efficient convolutional neural networks for mobile vision applications. *arXiv:1704.04861*, 2017. 3
- [30] Xu Jia, Bert De Brabandere, Tinne Tuytelaars, and Luc V Gool. Dynamic filter networks. *NeurIPS*, 2016. 1, 2, 3
- [31] Yifan Jiang, Shiyu Chang, and Zhangyang Wang. Transgan: Two pure transformers can make one strong gan, and that can scale up. *arXiv:2102.07074 v1*, 2021. 7
- [32] Yifan Jiang, Xinyu Gong, Ding Liu, Yu Cheng, Chen Fang, Xiaohui Shen, Jianchao Yang, Pan Zhou, and Zhangyang Wang. Enlightengan: Deep light enhancement without paired supervision. *IEEE Transactions on Image Processing*, 2021. 2

- [33] Hirokatsu Kataoka, Kazushige Okayasu, Asato Matsumoto, Eisuke Yamagata, Ryosuke Yamada, Nakamasa Inoue, Akio Nakamura, and Yutaka Satoh. Pre-training without natural images. *ACCV*, 2020. 2
- [34] Orest Kupyn, Volodymyr Budzan, Mykola Mykhailych, Dmytro Mishkin, and Jiří Matas. Deblurgan: Blind motion deblurring using conditional adversarial networks. *CVPR*, 2018. 2
- [35] Orest Kupyn, Tetiana Martyniuk, Junru Wu, and Zhangyang Wang. Deblurgan-v2: Deblurring (orders-of-magnitude) faster and better. *ICCV*, 2019. 2
- [36] Duo Li, Jie Hu, Changhu Wang, Xiangtai Li, Qi She, Lei Zhu, Tong Zhang, and Qifeng Chen. Involution: Inverting the inheritance of convolution for visual recognition. *CVPR*, 2021. 1, 2, 3, 8
- [37] Siyuan Li, Iago Breno Araujo, Wenqi Ren, Zhangyang Wang, Eric K Tokuda, Roberto Hirata Junior, Roberto Cesar-Junior, Jiawan Zhang, Xiaojie Guo, and Xiaochun Cao. Single image deraining: A comprehensive benchmark analysis. *CVPR*, 2019. 2
- [38] Jingyun Liang, Jie Zhang Cao, Guolei Sun, Kai Zhang, Luc Van Gool, and Radu Timofte. Swinir: Image restoration using swin transformer. *ICCV*, 2021. 2, 4, 5, 6, 7, 8
- [39] Jie Liang, Hui Zeng, and Lei Zhang. High-resolution photo-realistic image translation in real-time: A laplacian pyramid translation network. *CVPR*, 2021. 4
- [40] Bee Lim, Sanghyun Son, Heewon Kim, Seungjun Nah, and Kyoung Mu Lee. Enhanced deep residual networks for single image super-resolution. *CVPR workshops*, 2017. 2, 4
- [41] Xudong Lin, Lin Ma, Wei Liu, and Shih-Fu Chang. Context-gated convolution. *ECCV*, 2020. 3
- [42] Ze Liu, Yutong Lin, Yue Cao, Han Hu, Yixuan Wei, Zheng Zhang, Stephen Lin, and Baining Guo. Swin transformer: Hierarchical vision transformer using shifted windows. *arXiv:2103.14030*, 2021. 7
- [43] Kede Ma, Zhengfang Duanmu, Qingbo Wu, Zhou Wang, Hongwei Yong, Hongliang Li, and Lei Zhang. Waterloo exploration database: New challenges for image quality assessment models. *IEEE Transactions on Image Processing*, 2016. 4
- [44] Julien Mairal, Francis Bach, Jean Ponce, Guillermo Sapiro, and Andrew Zisserman. Non-local sparse models for image restoration. *ICCV*, 2009. 2
- [45] Ben Mildenhall, Jonathan T. Barron, Jiawen Chen, Dillon Sharlet, Ren Ng, and Robert Carroll. Burst denoising with kernel prediction networks. *CVPR*, 2018. 1, 3
- [46] Yali Peng, Lu Zhang, Shigang Liu, Xiaojun Wu, Yu Zhang, and Xili Wang. Dilated residual networks with symmetric skip connection for image denoising. *Neurocomputing*, 2019. 2, 5
- [47] Pietro Perona and Jitendra Malik. Scale-space and edge detection using anisotropic diffusion. *TPAMI*, 1990. 2
- [48] Gabriel Peyré, Sébastien Boleux, and Laurent Cohen. Non-local regularization of inverse problems. *ECCV*, 2008. 2
- [49] Dongwei Ren, Wangmeng Zuo, Qinghua Hu, Pengfei Zhu, and Deyu Meng. Progressive image deraining networks: A better and simpler baseline. *CVPR*, 2019. 2
- [50] Leonid I Rudin, Stanley Osher, and Emad Fatemi. Nonlinear total variation based noise removal algorithms. *Physica D: nonlinear phenomena*, 1992. 2
- [51] Mark Sandler, Andrew Howard, Menglong Zhu, Andrey Zhmoginov, and Liang-Chieh Chen. Mobilenetv2: Inverted residuals and linear bottlenecks. *CVPR*, 2018. 4
- [52] Wenzhe Shi, Jose Caballero, Ferenc Huszár, Johannes Totz, Andrew P Aitken, Rob Bishop, Daniel Rueckert, and Zehan Wang. Real-time single image and video super-resolution using an efficient sub-pixel convolutional neural network. In *Proceedings of the IEEE conference on computer vision and pattern recognition*, pages 1874–1883, 2016. 4
- [53] Xin Tao, Hongyun Gao, Xiaoyong Shen, Jue Wang, and Ji-aya Jia. Scale-recurrent network for deep image deblurring. *CVPR*, 2018. 2
- [54] Chunwei Tian, Yong Xu, and Wangmeng Zuo. Image denoising using deep cnn with batch renormalization. *Neural Networks*, 2020. 5
- [55] Ashish Vaswani, Noam Shazeer, Niki Parmar, Jakob Uszkoreit, Llion Jones, Aidan N Gomez, Łukasz Kaiser, and Illia Polosukhin. Attention is all you need. *NeurIPS*, 2017. 2
- [56] Jiaqi Wang, Kai Chen, Rui Xu, Ziwei Liu, Chen Change Loy, and Dahua Lin. Carafe: Content-aware reassembly of features. *ICCV*, 2019. 1, 3
- [57] Chen Wei, Wenjing Wang, Wenhan Yang, and Jiaying Liu. Deep retinex decomposition for low-light enhancement. *arXiv:1808.04560*, 2018. 2
- [58] Zhihao Xia and Ayan Chakrabarti. Identifying recurring patterns with deep neural networks for natural image denoising. *WACV*, 2020. 5
- [59] Yu-Syuan Xu, Shou-Yao Roy Tseng, Yu Tseng, Hsien-Kai Kuo, and Yi-Min Tsai. Unified dynamic convolutional network for super-resolution with variational degradations. *CVPR*, 2020. 1
- [60] Wenhan Yang, Robby T Tan, Shiqi Wang, Yuming Fang, and Jiaying Liu. Single image deraining: From model-based to data-driven and beyond. *TPAMI*, 2020. 2
- [61] Zongsheng Yue, Hongwei Yong, Qian Zhao, Lei Zhang, and Deyu Meng. Variational denoising network: Toward blind noise modeling and removal. *arXiv preprint arXiv:1908.11314*, 2019. 8
- [62] Syed Waqas Zamir, Aditya Arora, Salman Khan, Munawar Hayat, Fahad Shahbaz Khan, Ming-Hsuan Yang, and Ling Shao. Learning enriched features for real image restoration and enhancement. *ECCV*, 2020. 2, 4, 8
- [63] Syed Waqas Zamir, Aditya Arora, Salman Khan, Munawar Hayat, Fahad Shahbaz Khan, Ming-Hsuan Yang, and Ling Shao. Multi-stage progressive image restoration. *CVPR*, 2021. 2, 8
- [64] Kai Zhang, Yawei Li, Wangmeng Zuo, Lei Zhang, Luc Van Gool, and Radu Timofte. Plug-and-play image restoration with deep denoiser prior. *TPAMI*, 2021. 4, 5
- [65] Kai Zhang, Wangmeng Zuo, Yunjin Chen, Deyu Meng, and Lei Zhang. Beyond a gaussian denoiser: Residual learning of deep cnn for image denoising. *IEEE transactions on image processing*, 2017. 2, 5, 6, 7, 8

- [66] Kai Zhang, Wangmeng Zuo, Shuhang Gu, and Lei Zhang. Learning deep cnn denoiser prior for image restoration. *CVPR*, 2017. 5
- [67] Kai Zhang, Wangmeng Zuo, and Lei Zhang. Ffdnet: Toward a fast and flexible solution for cnn-based image denoising. *IEEE Transactions on Image Processing*, 2018. 5, 6
- [68] Lei Zhang, Xiaolin Wu, Antoni Buades, and Xin Li. Color demosaicking by local directional interpolation and nonlocal adaptive thresholding. *Journal of Electronic imaging*, 2011. 4
- [69] Yulun Zhang, Kunpeng Li, Kai Li, Bineng Zhong, and Yun Fu. Residual non-local attention networks for image restoration. *arXiv:1903.10082*, 2019. 2, 4, 5
- [70] Yulun Zhang, Yapeng Tian, Yu Kong, Bineng Zhong, and Yun Fu. Residual dense network for image super-resolution. *CVPR*, 2018. 2, 4, 5, 6, 7
- [71] Yulun Zhang, Donglai Wei, Can Qin, Huan Wang, Hanspeter Pfister, and Yun Fu. Context reasoning attention network for image super-resolution. *ICCV*, 2021. 3
- [72] Sixiao Zheng, Jiachen Lu, Hengshuang Zhao, Xiatian Zhu, Zekun Luo, Yabiao Wang, Yanwei Fu, Jianfeng Feng, Tao Xiang, Philip HS Torr, et al. Rethinking semantic segmentation from a sequence-to-sequence perspective with transformers. *CVPR*, 2021. 7

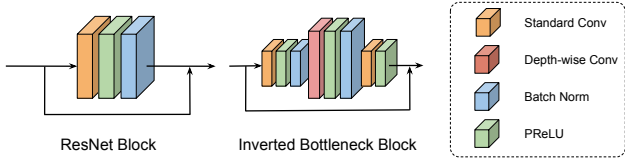


Figure 11. Detailed illustration of “ResNet Block” and “Inverted Bottleneck Block” used in the proposed MalleNet architecture.

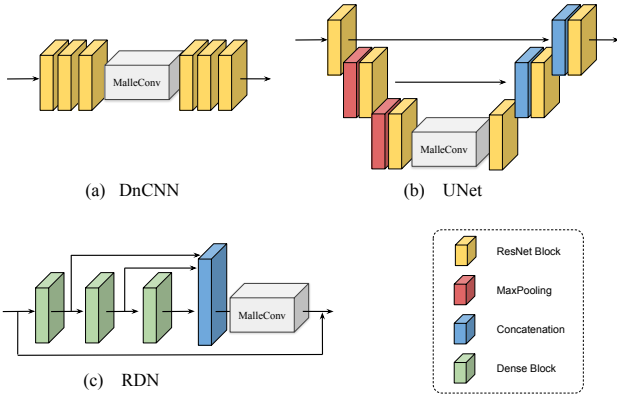


Figure 12. Detailed injected position of Malleable Convolution on different backbones.

A. Architecture Details

The proposed MalleNet-families include MalleNet-XS, -S, -M, -L, and -XL. We start from constructing MalleNet-XS. MalleNet-XS consists of four levels, the top two levels use 16-channel intermediate features and bottom two levels

use 32-channel intermediate features. We adopt standard ResNet Block as the basic operator for each level, whose detailed structure is shown in Fig. 12 left. We use two ResNet blocks for each of the top two levels and six ResNet blocks for each of the bottom two levels, the and inject one 3×3 MalleConv layer in the middle of each level.

To construct MalleNet-S, the standard ResNet Block is replaced by Inverse Bottleneck Block. The details of Inverse Bottleneck Block is presented in Fig. 12 right and we use a fixed expansion ratio of 3 in the depth-wise convolution. This modification will not make much affect on FLOPs number of whole network, but introduce additional runtime latency since depth-wise convolution is not a GPU-friendly operator, and extra performance improvement as well.

To construct MalleNet-M, -L, -XL, we simply modify MalleNet-S by growing the number of channels of each layer from $\{16, 16, 32, 32\}$ to $\{32, 32, 64, 64\}$, $\{64, 64, 128, 128\}$, $\{128, 128, 256, 256\}$ respectively. For MalleNet-XL, we further increase the expansion ratio from 3 to 5 to increase its capability. For real-world noise benchmark SIDD dataset, we construct MalleNet-R by adjusting the base channel number to 64 and adopt ResNet Block as basic operator, larger channel is observed to result in over-fitting issue.

To better illustrate how to adopt MalleConv on existing popular backbones, we describe the detailed injecting position of MalleConv in the ablation study on Sec. 5.2 of our main manuscripts. Concretely speaking, we inject MalleConv in the middle layer of DnCNN and UNet, and the last layer of Residual Dense Block (RDN). Furthermore, we present the details of the proposed efficient predictor network, as shown in Fig. 13. The predictor network is constructed with several stacked ResNet Blocks and Max-Pooling layer. We apply the standard ResNet blocks for all variants of MalleNet-families.

B. Visual Comparison

We include the visual comparisons between the proposed MalleNet and previous state-of-the-art approaches on both simulated benchmarks and real-world benchmark (SIDD), as shown in Fig. 14 and Fig. 15. Since SIDD only provide validation set with 256×256 patches as noisy/gt paired data, we report the PSNR/SSIM and visual results on validation set. As shown in Fig. 14, we randomly pick several visual examples generated from MalleNet-R and the best competitor HINet, and observe similar performance between these two approaches, although quantitative score provided by MalleNet-R slightly behinds the HINet. This might because the diminishing marginal utility of PSNR when it reaches an enough high value. Moreover, regarding to the efficiency, MalleNet-R saves up to $\times 2.42$ runtime latency and $\times 5.86$ FLOPs costs.

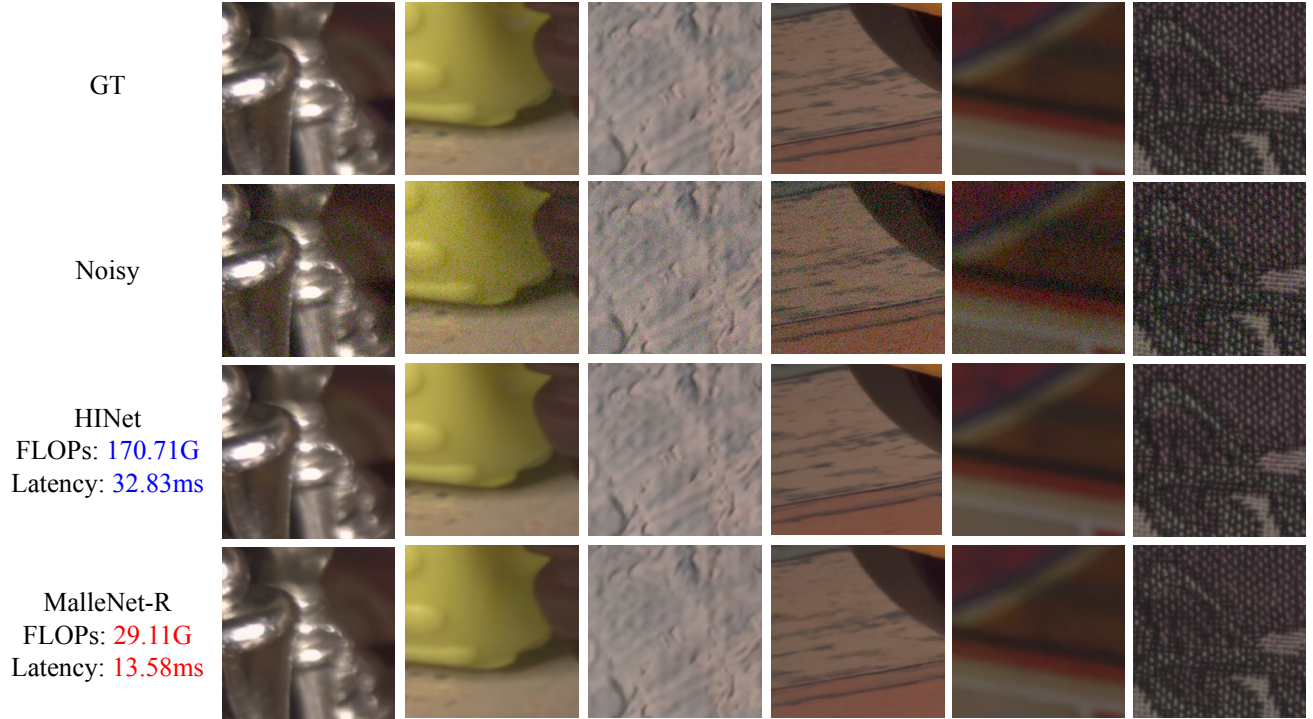
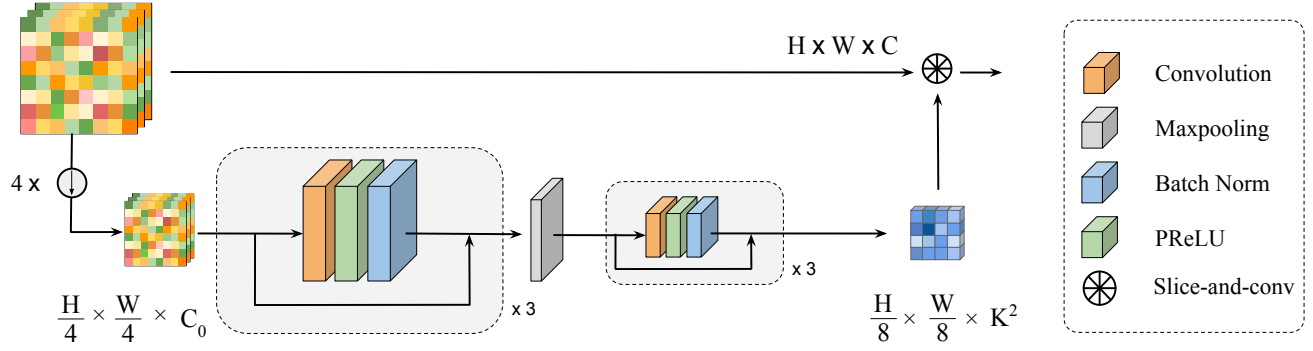


Figure 14. Randomly picked testing patches from MalleNet and previous state-of-the-art methods on real-world noise benchmark (SIDD). **Best viewed in color and zoomed in.**

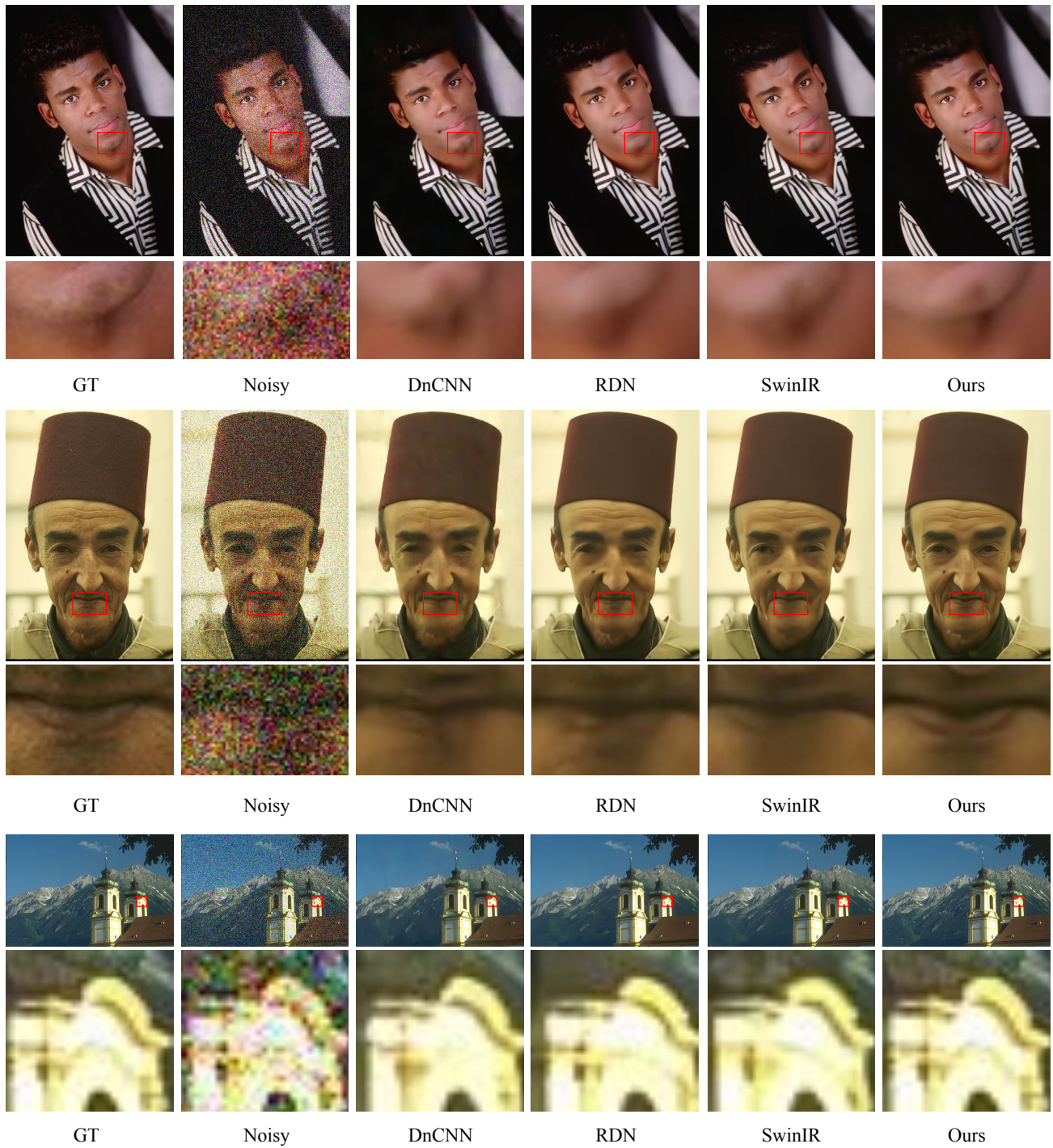


Figure 15. Visual Comparison between MalleNet and previous state-of-the-art methods on simulated dataset ($\sigma = 50$).